Space Debris Removal with Harpoon Assistance: Choice of Parameters and Optimization

Dmitry A. Sizov* and Vladimir S. Aslanov†

Samara National Research University, 443086, Samara, Russia

This paper discusses three phases of the space debris removal with harpoon assistance: capture, tether deployment, and towing. The harpoon impact momentum is used to detumble the target. Equations of motion for each phase are given in dimensionless form, which significantly reduces the number of parameters describing the system. The aim of the paper is to propose algorithms for choosing optimal parameters for the capture and tether deployment phases. This optimization provides small amplitudes of the tether and debris oscillations during towing. The numerical simulations of the removal of a spent Ariane 4 upper stage H10 confirm the correctness of the proposed mathematical models and optimization algorithms.

Nomenclature

a	=	dimensionless tug thrust
c_{ij}	=	dimensionless elements of Jacobian matrix
D	=	diameter of the target, m
d	=	distance between the tug and center of mass of the target, m
E_α	=	dimensionless total energy of the tether oscillations
E_β	=	dimensionless total energy of the target oscillations
h	=	dimensionless arm of the impact impulse
J_x	=	longitudinal moment of inertia of the target, $\text{kg} \cdot \text{m}^2$
J_y, J_z	=	transverse moments of inertia of the target, $\text{kg} \cdot \text{m}^2$
$\boldsymbol{J}$	=	dimensionless Jacobian matrix
KE	=	kinetic energy, J
k_α, k_β	=	dimensionless natural frequencies
k_1, k_2	=	elliptic moduli
l	=	tether length, m
m, m_1, m_2	=	mass, kg
n	=	mean motion of the center of mass of the target, rad/s
r_0	=	orbit radius, m
s	=	dimensionless impact impulse
T	=	dimensionless period of oscillations of the target
t	=	time, s
U	=	dimensionless potential energy of the tether oscillations
$\boldsymbol{u}$	=	vector of optimal tug thrust control law parameters
$\boldsymbol{v}$	=	eigenbasis of the linearized equations of the tethered towing
$\boldsymbol{w}$	=	vector of perturbed variables describing the tethered towing
x, y	=	coordinates of the relative motion of the tug, m
$\bar{x}, \bar{y}$	=	dimensionless coordinates of the relative motion of the tug
α	=	angle between the tether and local horizontal, rad
β	=	angle between the longitudinal axis of the target and local horizontal, rad
γ	=	harpoon obliquity angle, rad
Δ	=	dimensionless capture point shift parameter
Δ_L	=	dimensionless longitudinal shift of the capture point
Δ_T	=	dimensionless transverse shift of the capture point
δ	=	dimensionless distance between the tug and center of mass of the target
η	=	tug thrust direction angle, rad
θ	=	angle between the local horizontal and the line through the tug and the center of mass, rad
λ	=	vector of eigenvalues of the linearized equations of the tethered towing
μ	=	gravitational parameter of the Earth, $\text{m}^3 \cdot \text{s}^{-2}$
ν	=	true anomaly of the target, rad
τ	=	dimensionless time
ω	=	dimensionless angular frequency of the attitude motion of the free target

Subscripts

c	=	capture
h	=	harpoon
L	=	longitudinal
s	=	stable
T	=	transverse
u	=	unstable
1	=	tug
2	=	target
$-$	=	before capture
$+$	=	after capture

*Senior Researcher, Theoretical Mechanics Department, 34, Moscovskoe Shosse.

†Head of Department, Professor, Theoretical Mechanics Department, 34, Moscovskoe Shosse.

I. Introduction

THE continuing increase of the space debris population is threatening the future of space exploration [1]. For this reason, a significant number of space debris removal methods have been proposed and analyzed in recent years [2–4]. One of the most promising methods is to use space tether systems [5,6] for deorbiting space debris [7–13]. In the context of space debris removal, the principal components of the space tether system are the passive debris object (target), active spacecraft (tug), and capturing device, such as a net [14,15] or a harpoon. To study the possibility of using harpoons to capture space debris, both ground-based [16] and space experiments have been conducted recently. In early 2019, on the International Space Station, as part of the RemoveDebris project [17], a 10 cm by 10 cm aluminum honeycomb panel was captured by a harpoon from a distance of 1.5 m. Although the experiment was successful, real space debris objects may rotate, which may lead to the winding of the tether on the captured object during towing. To avoid this negative scenario, it is necessary to detumble the target beforehand. Several detumbling techniques have been recently proposed, including the use of tether

tension [18], eddy currents [19], or laser ablation [20]. The angular speed of the target can also be reduced due to the harpoon impact, but the influence of the capture parameters on the subsequent phases of the removal process is not fully investigated in this case. In addition, to ensure accurate targeting of the harpoon firing device, the tug must be close to the space debris object being captured, whereas for safe towing the tug must be placed at a significant distance. It is therefore necessary to further investigate the motion of the tug during the transition to the operating position after the capture. More generally, there are no studies that cover all phases of the space debris removal with harpoon assistance. Yet, it is important to consider this process as a whole, because each preceding phase affects the subsequent one. For instance, properly chosen capture parameters can provide a smaller amplitude of oscillations of the target during tethered towing.

The primary goal of the paper is therefore to discuss a more complete process of space debris removal with harpoon assistance and to propose algorithms for choosing the optimal parameters of the process. The secondary goal is to study the possibility of using the harpoon not only for capturing, but also for detumbling rotating space debris objects. To achieve these goals, the mathematical models of multiple phases of the removal process are proposed, the optimization of parameters of the process is performed, and numerical examples are considered.

The paper has the following structure. Section II deals with the separate phases of the removal process. In addition, the major challenges to be overcome during the mission planning are formulated. Section III presents mathematical models describing the motion of the system in each phase. Section IV is devoted to the selection of capture parameters and optimization of tug thrust control during tether deployment. Section V contains numerical examples of a spent upper stage removal. The final Sec. VI gives the conclusions.

II. Proposed Removal Technique and Related Challenges

The following method of space debris removal is proposed. The tug captures the target with a harpoon from a close distance, then moves to the position required for the towing, deploying the slack tether. The capture parameters are such that during the deployment time the target also moves to the position required for towing. Eventually, the tether is tensioned, and towing begins. The described process can be divided into three phases (Fig. 1), which are discussed in detail below.

The first phase includes the initial attitude motion of the target under the influence of the gravitational torque before the capture and the capture itself. The initial attitude motion of the target is characterized by some constant value of total mechanical energy, which changes instantly as a result of the harpoon impact. During this phase, the tug has to be close to the space debris object being captured at a distance that ensures sufficient targeting accuracy and at the same time prevents accidental collision with the object. Because the tug needs time to estimate the characteristics of the attitude motion of the object, select

the capture point and perform the targeting, the best relative position for the capture phase is when the tug is in the same orbit as the target. Depending on the direction of the initial rotation of the target, namely, in the direction of its mean orbital motion or the opposite direction, the tug may be placed behind or in front of the target.

In the second phase, the tug generates a thrust and moves away from the target, deploying the tether. It is assumed that during this process the tether is slack. This makes the design of the tug simpler, as no tether tension control device is required. Such a system is highly reliable because it has a minimal number of elements and does not require any tension control. At the same time, it will be necessary to control the tug thrust so that when the tether reaches the required length, the tug has the relative position and speed appropriate to start the towing. Note that during the tether deployment, the target will continue to rotate relative to its center of mass under the influence of the gravitational torque.

The third phase begins immediately after the tether deployment is complete. The tug changes the direction of the thrust, aligning it with the local horizontal, and starts the tethered towing of the target. It will be shown below that there exist equilibrium positions of the tether and the target about which they will oscillate during towing. The smaller are the amplitudes of these oscillations, the safer is the towing process. Small amplitudes can be achieved if after completion of the tether deployment both the tug and the target will be in strictly defined positions and have the specified velocities. It is therefore necessary to optimally choose not only the towing parameters, but also those of the relative motion of the tug during the tether deployment phase, as well as the capture parameters (see Sec. IV).

It can be expected that several challenges will arise during the planning of the described mission. In particular, for the capture phase, the following are necessary:

1) Assess the practical feasibility of using the harpoon impact for the detumbling of the particular target.

2) Choose the position of the tug relative to the target at the moment of capture.

3) Determine the required orientation of the target at the moment of capture and the location of the capture point.

For the tether deployment phase, the following are essential:

1) Find the relative position of the tug after completion of the tether deployment, providing the minimum amplitude of the tether oscillation in the subsequent towing phase.

2) Design the tug thrust control law that ensures that the tug reaches the above-mentioned position.

For the tethered towing phase, one must choose 1) the mass and amount of thrust of the tug and 2) the length of the tether.

The following sections are meant to solve these and other challenges related to the discussed space debris removal technique.

III. Dimensionless Equations of Motion

The equations of motion are derived in dimensionless form, which allows to investigate the behavior of the system in an arbitrary space
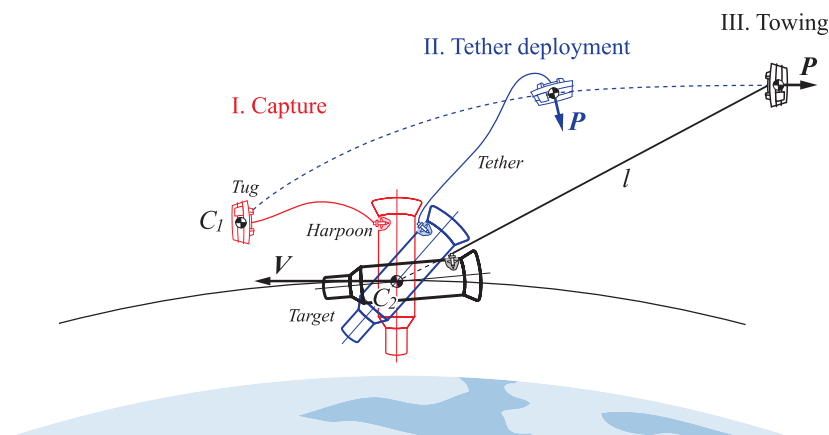

Fig. 1   Phases of space debris removal with harpoon assistance.

of parameters and formulate general recommendations. The equations of tethered towing are considered first, followed by the equations of relative motion of the tug, and finally the equations of attitude motion of the free target, including its motion during capture. Such order of presentation is because the parameters of the final phase must be taken into account while choosing the parameters of relative motion of the tug during the tether deployment phase, which, in their turn, have an influence on the capture parameters.

A. Main Assumptions

We impose the following assumptions.

1) The mass of the harpoon is small compared with the mass of the target.

2) The initial orbit of the target is circular ($r_0 =$ const), and the harpoon impact and tethered towing do not change its parameters. In this case, the true anomaly of the target ν can be used as a dimensionless time:

$$\tau \equiv \nu = nt \qquad (1)$$

where n is the mean motion:

$$n = \sqrt{\frac{\mu}{r_0^3}} = \text{const} \qquad (2)$$

μ is the gravitational parameter of the Earth.

3) The geometric, kinematic, and inertial parameters of the target are known.

4) The target has two equal principal moments of inertia ($J_y = J_z$, $J_z > J_x$).

5) All motions take place in the orbital plane of the target. This assumption is reasonable because after a long time in orbit, due to energy dissipation, space debris objects tend to rotate about the axis with the largest moment of inertia [21].

6) The tug is a point mass.

7) The tug thrust is directed along the local horizontal and its magnitude is constant.

8) The tether is massless and inextensible.

9) The tether properties are selected in a way that eliminates the risk of rupture during conventional towing, i.e., when the tether is not wrapped around the target.

10) The harpoon impact is modeled as a completely inelastic collision.

11) The influence of the atmosphere is negligible.

B. Tethered Towing

Following [13], let us write down the equations of motion for the tethered system in a circular orbit, which differ in that the capture point is placed arbitrarily on the sidewall of the target:
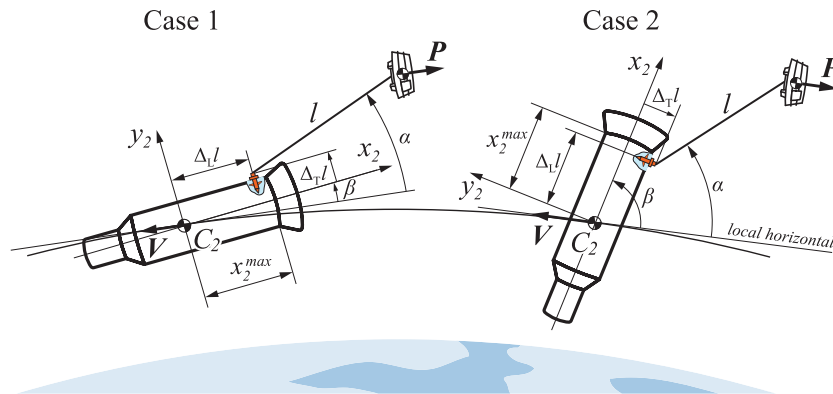
$$\alpha'' + [\Delta_L \cos(\alpha - \beta) + \Delta_T \sin(\alpha - \beta)]\beta''$$
$$+ (\beta'^2 + 2\beta')[\Delta_L \sin(\alpha - \beta) - \Delta_T \cos(\alpha - \beta)]$$
$$+ a \sin\alpha - \frac{3}{2}[\sin 2\alpha + 2\cos\alpha(\Delta_T \cos\beta + \Delta_L \sin\beta)] = 0 \qquad (3)$$

$$[\Delta_L \cos(\alpha - \beta) + \Delta_T \sin(\alpha - \beta)]\alpha'' + \left(\frac{J_z}{m_0 l^2} + \Delta_T^2 + \Delta_L^2\right)\beta''$$
$$- (\alpha'^2 + 2\alpha')[\Delta_L \sin(\alpha - \beta) - \Delta_T \cos(\alpha - \beta)]$$
$$+ a(\Delta_T \cos\beta + \Delta_L \sin\beta) + \frac{3}{2}\left(\Delta_T^2 - \Delta_L^2 + \frac{J_x - J_z}{m_0 l^2}\right)\sin 2\beta$$
$$- 3[\Delta_T \Delta_L \cos 2\beta + \sin\alpha(\Delta_L \cos\beta - \Delta_T \sin\beta)] = 0 \qquad (4)$$

where Δ_T and Δ_L are, respectively, the transverse and longitudinal shifts of the harpoon impact point from the center of the mass of the object, divided by the length of the tether l (Fig. 2); ( )$'$ means differentiation with respect to the dimensionless time τ; α is the angle between the local horizontal and the tether; β is the angle between the local horizontal and the longitudinal axis of the target; m_1 is the mass of the tug; m_2 is the mass of the target, $m_0 = m_1 m_2/(m_1 + m_2)$; J_x and J_z are the longitudinal and transverse principal moments of inertia of the target, respectively; and a is a dimensionless parameter [9], which can be interpreted as the dimensionless tug thrust:

$$a = \frac{P}{l m_1 n^2} \qquad (5)$$

where P is the tug thrust magnitude.

With the additional assumptions that the tether and target oscillations are small and the shift of the harpoon impact point from the center of mass of the target is small compared with the tether length, Eqs. (3) and (4) take the form

$$\alpha'' = -a \sin\alpha + \frac{3}{2}\sin 2\alpha \qquad (6)$$

$$\beta'' = \frac{1}{\hat{J}}\Delta_T(\Delta \sin(\alpha - \beta) - \cos(\alpha - \beta))(a \cos\alpha + 3\sin^2\alpha)$$
$$+ \frac{1}{2\tilde{J}}\sin 2\beta \qquad (7)$$

where $\hat{J}$, $\tilde{J}$, and Δ are dimensionless parameters:

$$\hat{J} = \frac{J_z}{m_0 l^2}, \quad \tilde{J} = \frac{J_z}{3(J_z - J_x)}, \quad \Delta = \frac{\Delta_L}{\Delta_T} \qquad (8)$$

It is supposed in Eq. (8) that $\Delta_T \neq 0$, since the proposed removal technique implies that the capture point is shifted from the longitudinal axis of the object. Note that there exist two different capture cases. In the first case, the coordinate $y_2 = \Delta_T l$ of the tether attachment point is
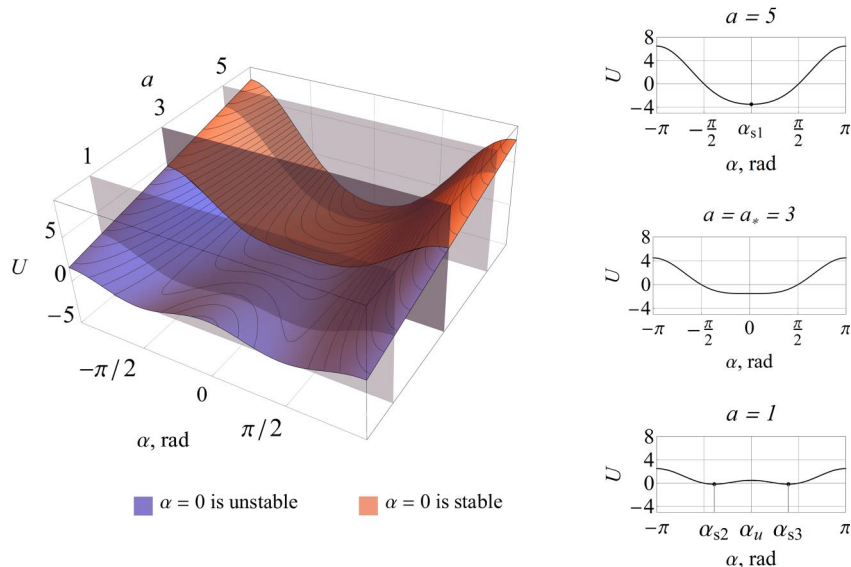

Fig. 2 Two cases of tethered towing of the target.

Fig. 3 Dimensionless potential energy of the unperturbed angular motion of the tether.

positive in the coordinate frame $C_2 x_2 y_2$ associated with the target (Fig. 2, left). Accordingly, the parameters Δ_T and Δ have the same sign. In the second case (Fig. 2, right), the parameters Δ_T and Δ are negative. All equations in this and the following sections are suitable for both capture cases provided that the sign of these parameters is taken into account. Note that the discussed capture cases are fundamentally different. Transition from one to another is only possible if the target rotates about its longitudinal axis x_2, which is beyond the scope of this paper.

Equations (6) and (7) give some physical insight into the motion of the tethered system. The tether oscillations are mainly caused by two torques: one due to the tug thrust and one due to the gravitational forces acting on the tug and the target. These torques are represented by the first and the second terms in the right-hand side of Eq. (6), respectively. Similarly, the oscillations of the target are also mainly caused by two torques: one due to the tether tension and one due to the gravity gradient. These torques are represented by the first and the second terms in the right-hand side of Eq. (7), respectively. The tension force itself is the factor $(a \cos \alpha + 3 \sin^2 \alpha)$ in the first term. Because the dimensionless tug thrust a is taken positive, for all values of α in the interval from $-\pi/2$ to $\pi/2$ corresponding to the conventional towing the tension force is positive; thus, the tether is always tensioned.

Equation (6) can be regarded as the equation of the unperturbed angular motion of the tensioned tether. Because both torques in its right-hand side depend only on the orientation of the tether, the dimensionless total mechanical energy of the unperturbed angular motion of the tether is conserved:

$$E_\alpha(\alpha, \alpha') = \frac{1}{2}\alpha'^2 + U(\alpha) = U(\alpha_m) = \text{const} \qquad (9)$$

where U is the dimensionless potential energy of the unperturbed motion of the tether,

$$U = -a \cos \alpha + \frac{3}{2}\cos^2 \alpha \qquad (10)$$

α_m is the amplitude, which corresponds to the equality

$$E_\alpha(\alpha, \alpha') = E_\alpha(\alpha_m, \alpha' = 0) \qquad (11)$$

The equilibrium positions of the tether α_i are the roots of the equation

$$\frac{\partial U}{\partial \alpha} = 0 \qquad (12)$$

$$\alpha_1 = 0, \qquad \alpha_{2,3} = \mp \arccos \frac{a}{3} \qquad (13)$$

When

$$\left.\frac{\partial^2 U}{\partial \alpha^2}\right|_{\alpha=\alpha_i} > 0 \qquad (14)$$

the potential energy is in its minimum and the equilibrium is stable. On the contrary, when

$$\left.\frac{\partial^2 U}{\partial \alpha^2}\right|_{\alpha=\alpha_i} < 0 \qquad (15)$$

the potential energy is in its maximum so the equilibrium is unstable. These cases are illustrated by the Fig. 3, which represents the dependency of the potential energy on the dimensionless thrust a and angle α. It can be seen that, when the parameter a is large, there exists one stable position $\alpha = \alpha_{s1} = 0$ (Fig. 3, top right). When a is small, there are two stable equilibrium positions, at the points $\alpha_{s2,3}$, while the point $\alpha = \alpha_u = 0$ becomes unstable (Fig. 3, bottom right). Solving the equation

$$\left.\frac{\partial^2 U}{\partial \alpha^2}\right|_{\alpha=0} = 0 \qquad (16)$$

one can find that the bifurcation point is at $a_* = 3$. The potential energy curve for this particular case is given in Fig. 3, middle right.

The evolution of the equilibrium positions of the tether can be represented more clearly by the bifurcation diagram (Fig. 4). When $a \geq 3$ the torque due to the tug thrust makes a greater contribution to
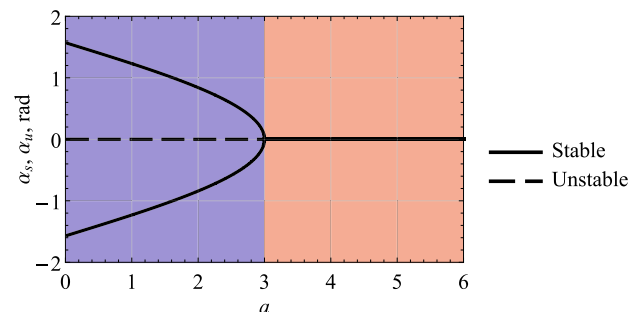

Fig. 4 Bifurcation diagram.

the static stability of the tether. As this torque tends to align the tether along the local horizontal, the point $\alpha = 0$ is stable. After passing the bifurcation point, the torque due to gravity, which tends to align the tether along the local vertical, becomes more significant, and the horizontal orientation of the tether is no longer stable. Equation (17) summarizes the above considerations about the stable equilibrium positions of the tether:

$$\alpha_s = \begin{cases} \pm \arccos\left(\dfrac{a}{3}\right), & a < 3, \\ 0, & a \geq 3 \end{cases} \qquad (17)$$

This means that if $a \geq 3$ the tug must be on the local horizontal of the target, whereas if $a < 3$ the tug must be above or below it. Note that Eq. (6), as well as the positions of the stable equilibrium of the tether (17), were introduced in [9].

For the given value of E_α, the amplitude of tether oscillations in the vicinity of the specified positions of stable equilibrium is

$$\alpha_m = \begin{cases} \dfrac{1}{2}(f_1(a, E_\alpha) - f_2(a, E_\alpha)), & E_\alpha < U_0, \\ 2f_1(a, E_\alpha), & E_\alpha > U_0 \end{cases} \qquad (18)$$

where

$$U_0 = U(0) \qquad (19)$$

$$f_{1,2} = \arccos \frac{\mp a + \sqrt{a^2 + 6E_\alpha}}{3} \qquad (20)$$

The first of the expressions (18) corresponds to oscillations in the vicinity of the positions $\alpha_{s2,3}$, whereas the second corresponds to oscillations near $\alpha_{s1} = 0$.

Let us find the equilibrium positions of the target that are characterized by the equality $\beta'' = \beta' = 0$. It is problematic to obtain the exact analytical expressions for the equilibrium positions from Eq. (7), but they can be found approximately as follows. As it was mentioned above, the acceleration β'' is influenced by two torques: one due to the tether tension, and the other one caused by the gravity gradient. Neglecting the gravitational torque, as it is small compared with the first one (Fig. 17), and equating Eq. (7) to zero, one can approximately find the equilibrium positions of the target:

$$\beta_0 = \alpha_s - \arctan\frac{\Delta_T}{\Delta_L} = \alpha_s - \arctan\frac{1}{\Delta} \qquad (21)$$

Clearly, β_0 corresponds to the position of the target at which its center of mass is on the same straight line as the tensioned tether. In reality, the gravitational moment will deflect the target from this position by a small angle, and a more accurate expression for the equilibrium positions is

$$\beta_s = \beta_0 + \beta_1 \qquad (22)$$

where the small angle β_1 can be found by expanding the right-hand side of Eq. (7) in the Taylor series in the vicinity of $\beta = \beta_0$ and equating the obtained expression to zero:

To find the natural frequencies of the tether and the target oscillations, we linearize Eqs. (6) and (7) in the vicinity of the obtained equilibrium positions (17) and (22) using new variables:

$$\delta\alpha = \alpha - \alpha_s, \quad \delta\beta = \beta - \beta_s \qquad (24)$$

Since α_s and β_s are constants,

$$\begin{aligned} \dot{\alpha} &= \delta\dot{\alpha}, & \ddot{\alpha} &= \delta\ddot{\alpha}, \\ \dot{\beta} &= \delta\dot{\beta}, & \ddot{\beta} &= \delta\ddot{\beta} \end{aligned} \qquad (25)$$

and, taking into account Eq. (25), we can write Eqs. (6) and (7) in the linearized form

$$\dot{\boldsymbol{w}} = \boldsymbol{J}\boldsymbol{w} \qquad (26)$$

where $\boldsymbol{w}$ is the vector of variables:

$$\boldsymbol{w} = [w_1 \quad w_2 \quad w_3 \quad w_4]^T = [\delta\alpha \quad \delta\dot{\alpha} \quad \delta\beta \quad \delta\dot{\beta}]^T \qquad (27)$$

$\boldsymbol{J}$ is the Jacobian matrix:

$$\boldsymbol{J} = \begin{pmatrix} 0 & 1 & 0 & 0 \\ c_{21} & 0 & 0 & 0 \\ 0 & 0 & 0 & 1 \\ c_{41} & 0 & c_{43} & 0 \end{pmatrix} \qquad (28)$$

where

$$c_{21} = -a\cos\alpha_s + 3\cos 2\alpha_s \qquad (29)$$

$$\begin{aligned} c_{41} &= \frac{1}{\hat{J}}\Delta_T(\Delta\cos(\alpha_s - \beta_s) + \sin(\alpha_s - \beta_s))(a\cos\alpha_s + 3\sin^2\alpha_s) \\ &+ \frac{1}{\hat{J}}\Delta_T(\cos(\alpha_s - \beta_s) - \Delta\sin(\alpha_s - \beta_s))(a - 6\cos\alpha_s)\sin\alpha_s \end{aligned} \qquad (30)$$

$$\begin{aligned} c_{43} &= \frac{\cos 2\beta_s}{\hat{J}} - \frac{1}{\hat{J}}\Delta_T(\Delta\cos(\alpha_s - \beta_s) + \sin(\alpha_s - \beta_s)) \\ &\times (a\cos\alpha_s + 3\sin^2\alpha_s) \end{aligned} \qquad (31)$$

The solution of the Eq. (26) has the form

$$\boldsymbol{w}(\tau) = \sum_{j=1}^{4} C_j e^{\lambda_j \tau} v_j \qquad (32)$$

where C_j are arbitrary constants, and v_j are the elements of the eigenbasis $\boldsymbol{v}$ of the system:

$$\boldsymbol{v} = [v_1 \quad v_2 \quad v_3 \quad v_4]^T \qquad (33)$$

with associated eigenvalues $\boldsymbol{\lambda}$:

$$\boldsymbol{\lambda} = [\lambda_1 \quad \lambda_2 \quad \lambda_3 \quad \lambda_4]^T \qquad (34)$$

which are pairs of conjugated complex numbers with zero real parts. The natural frequencies of the system are equal to the magnitudes of the imaginary parts of each pair of eigenvalues $\boldsymbol{\lambda}$. With Eqs. (28–31) taken into account, the natural frequencies are

$$\beta_1 = \frac{\tilde{J}\Delta_T(\cos(\alpha_s - \beta_0) - \Delta\sin(\alpha_s - \beta_0))(a\cos\alpha_s + 3\sin^2\alpha_s) - (\hat{J}/2)\sin 2\beta_0}{\hat{J}\cos 2\beta_0 - \tilde{J}\Delta_T(\Delta\cos(\alpha_s - \beta_0) + \sin(\alpha_s - \beta_0))(a\cos\alpha_s + 3\sin^2\alpha_s)} \qquad (23)$$

$$k_\alpha = \sqrt{a \cos \alpha_s - 3 \cos \alpha_s} \qquad (35)$$

$$k_\beta = \sqrt{\frac{\Delta_T[\Delta \cos(\alpha_s - \beta_s) + \sin(\alpha_s - \beta_s)][a\cos\alpha_s + 3\sin^2\alpha_s]}{\hat{J}} - \frac{\cos 2\beta_s}{\tilde{J}}} \qquad (36)$$

The approximate expressions for these frequencies with Eqs. (17) and (21) taken into account are

$$k_\alpha = \begin{cases} 3^{-(1/2)}\sqrt{9 - a^2}, & a < 3, \\ \sqrt{a - 3}, & a > 3 \end{cases} \qquad (37)$$

$$k_\beta = \begin{cases} \sqrt{\dfrac{3\Delta_L\sqrt{1 + (1/\Delta^2)}}{\hat{J}} - \dfrac{(2a^2 - 9)(\Delta^2 - 1) + 4a\Delta\sqrt{9 - a^2}}{9\hat{J}(\Delta^2 + 1)}}, & a < 3, \\ \sqrt{\dfrac{\Delta_T a \sqrt{\Delta^2 + 1}}{\hat{J}} - \dfrac{\Delta^2 - 1}{\hat{J}(\Delta^2 + 1)}}, & a > 3 \end{cases} \qquad (38)$$

C. Relative Motion of the Tug During Tether Deployment

The motion of one point mass relative to another point mass placed in a circular orbit is usually described by the Hill–Clohessy–Wiltshire equations given, e.g., in Ref. [22]:

$$\ddot{x} = 3n^2 x + 2n\dot{y} + a_x \qquad (39)$$

$$\ddot{y} = -2n\dot{x} + a_y \qquad (40)$$

For the problem under consideration, x and y are the coordinates of the tug relative to the center of the mass of the target (Fig. 5), and a_x and a_y are the radial and tangent components of the tug acceleration, respectively,

$$a_x = -\frac{P}{m_1} \cos \eta, \qquad a_y = -\frac{P}{m_1} \sin \eta \qquad (41)$$

where η is the thrust direction angle measured between the thrust vector and the local vertical.

Equations (39) and (40) can be presented in dimensionless form by dividing both sides of each equation by $n^2 l$:

$$\bar{x}'' = 3\bar{x} + 2\bar{y}' - a \cos \eta \qquad (42)$$

$$\bar{y}'' = -2\bar{x}' - a \sin \eta \qquad (43)$$

where

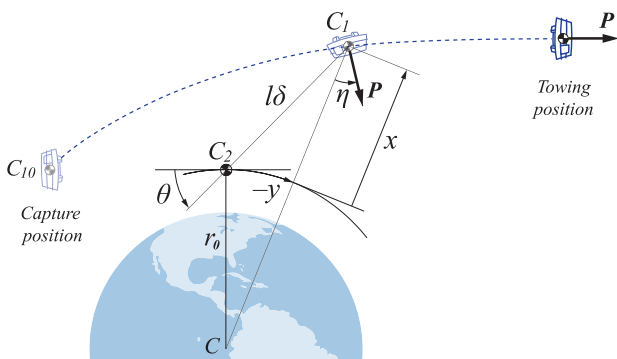$$\bar{x} = \frac{x}{l}, \qquad \bar{y} = \frac{y}{l} \qquad (44)$$

Fig. 5   Motion of the tug relative to the center of mass of the target C_2 during tether deployment.

Note that the relative motion of the tug also depends on the dimensionless thrust a introduced in the tethered towing Eqs. (3) and (4) and defined by Eq. (5).

If the thrust direction angle η is constant, Eqs. (42) and (43) have the following analytical solution:

$$\bar{x}(\tau) = (4 - 3\cos\tau)\bar{x}_0 + \bar{x}_0' \sin\tau - 2\bar{y}_0'(\cos\tau - 1) \\ + a(2\sin\eta(\sin\tau - \tau) + \cos\eta(\cos\tau - 1)) \qquad (45)$$

$$\bar{y}(\tau) = \bar{y}_0 + 6\bar{x}_0(\sin\tau - \tau) + \bar{y}_0'(4\sin\tau - 3\tau) + 2\bar{x}_0'(\cos\tau - 1) \\ + a\left(2\cos\eta(\tau - \sin\tau) + \frac{1}{2}(3\tau^2 + 8\cos\tau - 8)\sin\eta\right) \qquad (46)$$

where $\bar{x}_0$, $\bar{y}_0$, $\bar{x}_0'$, and $\bar{y}_0'$ are the initial conditions. Note that if $a = 0$ Eqs. (45) and (46) give the well-known solutions of the homogeneous equations of relative motion (see, e.g., [22]). In our case, at the initial moment the tug is in the same orbit as the target, so

$$\bar{x}_0 = \bar{x}_0' = \bar{y}_0' = 0 \qquad (47)$$

and the solutions (45) and (46) take the form

$$\bar{x}(\tau) = a(2\sin\eta(\sin\tau - \tau) + \cos\eta(\cos\tau - 1)) \qquad (48)$$

$$\bar{y}(\tau) = \bar{y}_0 + a\left(2\cos\eta(\tau - \sin\tau) + \frac{1}{2}(3\tau^2 + 8\cos\tau - 8)\sin\eta\right) \qquad (49)$$

In the tether deployment phase, it is essential to track the distance between the center of mass of the target and the tug. This distance can be expressed in terms of $\bar{x}$ and $\bar{y}$. To do this, we need to introduce the polar coordinates, namely, the angle θ between the local horizontal and the line connecting the tug and the center of mass of the target (Fig. 5) and the dimensionless distance δ between the tug and the center of mass of the target,

$$\delta = \frac{d}{l} \qquad (50)$$

where d is the distance between the tug and the center of mass of the target. If this distance is small compared with the orbit radius, the following equations apply:

$$\bar{x} = \delta \sin\theta, \qquad \bar{y} = -\delta \cos\theta \qquad (51)$$

Taking into account Eq. (51), we can find the analytical expressions for the functions $\theta(\tau)$ and $\delta(\tau)$:

$$\theta(\tau) = -\arctan\frac{\bar{x}(\tau)}{\bar{y}(\tau)} \qquad (52)$$

$$\delta(\tau) = \sqrt{\bar{x}^2(\tau) + \bar{y}^2(\tau)} \qquad (53)$$

where $\bar{x}(\tau)$ and $\bar{y}(\tau)$ are defined by Eqs. (48) and (49). Because the offset of the tether attachment point from the center of the mass of the target is small compared with the length of the tether, it can be stated that the tether deployment phase ends when $\delta = 1$. At this moment, the tether becomes tensioned, so the initial values of the variables α and α' characterizing the tether oscillations during towing are equal to the final values of the variables θ and θ'.

D. Attitude Motion of the Target

The considered method of removal implies that, before the capture, the target rotates in the orbital plane, and immediately after the capture the target begins to oscillate. Both cases are described by a well-known equation:

$$J_z\ddot{\beta} = \frac{3}{2}n^2(J_z - J_x)\sin 2\beta \qquad (54)$$

which can be written in dimensionless form taking Eq. (8) into account:

$$\beta'' = \frac{1}{2\tilde{J}}\sin 2\beta \qquad (55)$$

Note that this equation can also be obtained from Eq. (7) by equating to zero the first term in the right-hand side, which represents the torque due to the tether tension. Equation (55) has an energy integral, which can be written as

$$E_\beta = \frac{1}{2}\tilde{J}\beta'^2 + \frac{1}{2}\cos^2\beta = \text{const} \qquad (56)$$

The total energy corresponding to the separatrix is independent of $\tilde{J}$ and is equal to $1/2$. If $E_\beta < 1/2$, the target oscillates; if $E_\beta > 1/2$, it rotates.

Let us reduce Eq. (55) to the pendulum equation by introducing a new variable

$$\varphi = 2\beta - \pi \qquad (57)$$

Substituting Eq. (57) into Eq. (55) we obtain the nonlinear pendulum equation

$$\varphi'' = -\omega^2 \sin\varphi \qquad (58)$$

where

$$\omega = \frac{1}{\sqrt{\tilde{J}}} \qquad (59)$$

Note that in the discussed problem the target may significantly deviate from the stable equilibrium positions, so the linearization of Eq. (58) is impractical.

Equation (58) has well-known analytical solutions [23]. For the rotation case with initial conditions $\varphi(0) = 0$ and $\varphi'(0) = \varphi'_0$ the solution has the form

$$\varphi(\tau) = 2am\left(\frac{\varphi'_0}{2}\tau, k_1\right) \qquad (60)$$

where am is the Jacobi amplitude with the elliptic modulus k_1,

$$k_1 = 2\frac{\omega}{\varphi'_0} \qquad (61)$$

For the rotation case with arbitrary initial conditions the solution can be written as

$$\varphi(\tau) = 2\arcsin[k_2 sn(\omega(\tau + \tau_c), k_2)] \qquad (62)$$

where sn is the elliptic sine, and k_2 and τ_c are parameters depending on initial conditions. The elliptic modulus k_2 in our case can be defined as

$$k_2 = \sin\left(\frac{\varphi_{\max}}{2}\right) \qquad (63)$$

where, according to Eq. (57),

$$\varphi_{\max} = 2\beta_s - \pi \qquad (64)$$

and β_s is the required final position of the target, determined by Eq. (22). The period of oscillations is

$$T = \frac{4K(k_2)}{\omega} \qquad (65)$$

where K is the complete elliptic integral of the first kind. The time τ_c required for the target to move from its equilibrium position at $\varphi = 0$ to a displacement of $\varphi = \varphi_c$ at the moment of capture can be found as

$$\tau_c = \frac{1}{\omega}F(\psi_c, k_2) \qquad (66)$$

where F is the incomplete elliptic integral of the first kind:

$$\psi_c = \arcsin\left[\frac{1}{k_2}\sin\left(\frac{\varphi_c}{2}\right)\right] \qquad (67)$$

After backsubstitution according to Eq. (57), Eqs. (60) and (62), respectively, describe the motion of the free target before and after the capture, up to the moment when the tether is tensioned.

The initial conditions for Eq. (62) must be chosen bearing in mind that the harpoon impact instantly changes the angular speed of the target. In dimensionless form, this change can be represented as follows:

$$\beta'_+ = \beta'_- - \text{sgn}(\beta'_-)hs \qquad (68)$$

where β'_- is the angular speed of the target just before the harpoon impact, β'_+ is the angular speed just after the impact, s is a dimensionless parameter, proportional to the initial momentum of the harpoon $m_h v_h$,

$$s = \frac{m_h v_h l}{J_z n} \qquad (69)$$

m_h is the mass of the harpoon, v_h is the initial speed of the harpoon relative to the target, and h is the dimensionless arm of the impact momentum. This parameter is visualized in Fig. 6 along with other capture parameters for two capture cases discussed in Sec. III.B.
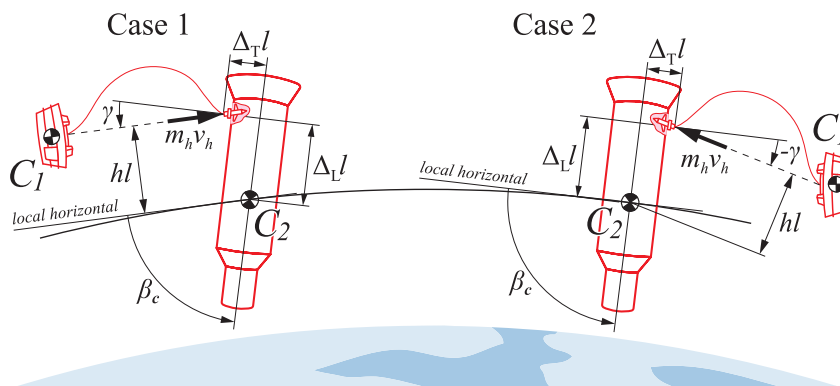

Fig. 6 Harpoon capture of space debris.

Within the assumption that the tug and the target are in the same orbit and the impact point shift from the center of mass of the target is small compared with the initial distance between the tug and the target, the dimensionless arm of the impact momentum can be defined as

$$h = \Delta_T(\Delta \sin \beta_c + \cos \beta_c) \qquad (70)$$

where β_c characterizes the orientation of the target at the moment of capture. Using the same assumption, one can determine the angle of obliquity (Fig. 6) as

$$\gamma = \begin{cases} \dfrac{\pi}{2} - \beta_c, & \beta_c \leq \dfrac{\pi}{2}, \\[2mm] \beta_c - \dfrac{\pi}{2}, & \beta_c > \dfrac{\pi}{2} \end{cases} \qquad (71)$$

IV. Optimization of the Removal Process

This section provides methods for choosing the parameters of the system minimizing the amplitudes of the tether and target oscillations during tethered towing. Minimization of the tether oscillations amplitude is performed by choosing the parameters of the tug thrust direction control law used in the tether deployment phase. Minimization of the target oscillation amplitude is performed primarily by choosing the position of the capture point, as well as by choosing the dimensionless parameter $a = P/(lm_1 n^2)$, characterizing the combination of the tug thrust magnitude, tug mass, and tether length.

A. Optimal Tug Thrust Direction Control During Tether Deployment

This subsection aims to choose the tug thrust direction control law for the tether deployment phase, which provides small amplitude of tether oscillations in the towing phase. To minimize the amplitude α_m, it is sufficient to minimize the total energy of the tether oscillations

$$E_\alpha(\alpha_0, \alpha_0') = U(\alpha_m) \rightarrow \min \qquad (72)$$

where $\alpha_0 \equiv \theta(\tau_2)$ and $\alpha_0' \equiv \theta'(\tau_2)$ are, respectively, the position and dimensionless angular speed of the tether at the moment τ_2, when the towing starts or, which is the same, when the tether deployment is completed. In the ideal case, $\alpha_0 = \alpha_s$ and $\alpha_0' = 0$; i.e., the tug completes the deployment when the tether is in one of its equilibrium positions (17).

There are some constraints to keep in mind when minimizing the cost function (72). Firstly, at the moment τ_2 the tether must be fully deployed. Secondly, we consider unsafe, and therefore unacceptable, the situation when the tug approaches the target closer than half of the initial distance δ_0. Thirdly, when the tether is fully deployed, the tug must be moving away from the target at a speed that cannot cause the tether rupture. The described constraints can be mathematically formulated in the following way:

$$\begin{aligned} &\delta(\tau_2) = 1, \\ &\delta(\tau) \geq \frac{\delta_0}{2}, \\ &0 \leq \delta'(\tau_2) \leq \delta'_{\max} \end{aligned} \qquad (73)$$

where $\delta'_{\max}$ is the maximum allowed value of the longitudinal component of the tug relative speed at the moment when the tether becomes tensioned.

We take one of the possible tug thrust direction control laws, which has a simple form

$$\eta(\tau) = \begin{cases} \eta_1, & \tau \leq \tau_1, \\ \eta_2, & \tau_1 < \tau \leq \tau_2 \end{cases} \qquad (74)$$

where τ_1 is the moment of dimensionless time at which the thrust direction angle (Fig. 5) changes from η_1 to η_2. If the thrust magnitude remains constant, this change of direction is necessary because the tug must first accelerate relative to the target and then come to a stop.

The solution to the optimization problem under consideration is the vector

$$\boldsymbol{u} = \begin{bmatrix} \eta_1 & \tau_1 & \eta_2 & \tau_2 \end{bmatrix}^T \qquad (75)$$

minimizing the cost function Eq. (72) and satisfying the constraints Eq. (73).

According to Eq. (74), the relative motion of the tug is divided into two phases. During each phase, the thrust direction angle η remains constant, so the time histories of the tug polar coordinates θ and δ are described by Eqs. (52) and (53), respectively, and the time histories of the speeds θ' and δ' are simply the time derivatives of these analytical expressions. The values of these variables at the end of the first phase of the relative motion must be used as the initial conditions for the second phase.

As it can be seen from Eqs. (42) and (43), the relative motion of the tug largely depends on the dimensionless thrust a, so it is necessary to find the function $\boldsymbol{u}(a)$. Figure 7 depicts an example of such a dependency, obtained as a result of the minimization of the cost function Eq. (72) using simulated annealing method [24]. It is worth mentioning that as the tug is initially at rest relative to the target and $\delta_0 \ll \delta(\tau_2)$, the initial conditions θ_0 and δ_0 have little influence on the optimal values of control parameters. Figure 7 also shows approximate values of the amplitudes of tether oscillations calculated using Eq. (18). It can be seen that for the chosen initial conditions and the tug final speed limit the amplitude of tether oscillations will be small if $a > 1.95$. Figure 8 shows the relative trajectories of the tug corresponding to different values of the parameter a. It can be observed that in all cases considered the tug moves up relative to the target, although according to Eq. (17) there is also an equilibrium position when the tug is placed below the target. This alternative is not covered here, because numerical simulations show that, taking into account the constraints (73), placing the tug below the target is only feasible in a very narrow range of a.
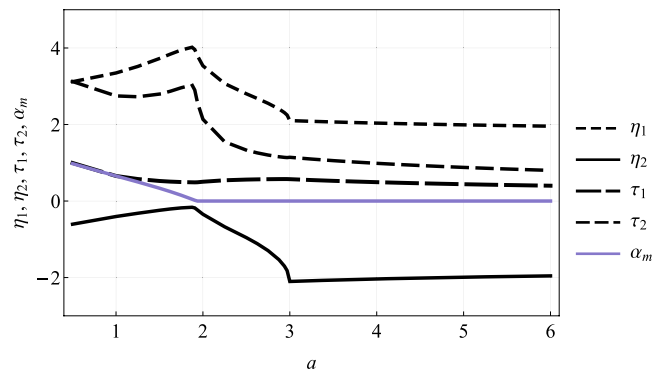
Fig. 7   Optimal tug thrust direction control parameters for the tether deployment phase and corresponding amplitudes of tether oscillations ($\theta_0 = 0$, $\delta_0 = 0.06$, $\delta'_{\max} = 0.02$).
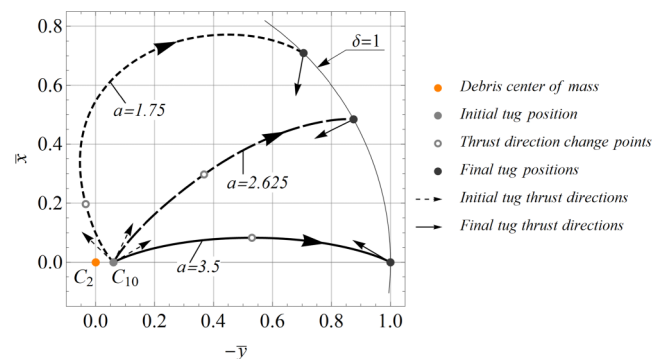
Fig. 8   Examples of relative trajectories of the tug during tether deployment ($\theta_0 = 0$, $\delta_0 = 0.06$, $\delta'_{\max} = 0.02$).

Thus, it is shown that for the given initial conditions and the tug final speed limit one can find the dependencies of optimal control parameters on the dimensionless thrust a. These dependencies give some idea of the values of the parameter that provide small amplitude of tether oscillations during the towing phase. However, the final choice of this parameter has to be made during the analysis of the capture, which is considered in the next subsection.

B. Choice of Capture Parameters

The aim of this subsection is to choose the orientation of the target at the moment of capture β_c as well as the values of the capture point longitudinal shift Δ and dimensionless thrust a. The correct choice of these quantities allows to solve the following challenges. Firstly, the probability of full penetration of the target shell has to be maximized. Secondly, precisely at the moment τ_2, when the tether deployment is complete, the target must stop at the equilibrium position β_s [Eq. (22)], which will reduce the amplitude of its oscillations during towing.

It is shown in [16] that if the angle of obliquity (71) is large, the harpoon may slide along the surface without penetrating it. Therefore, in order to maximize the probability of successful capture, the velocity vector of the harpoon must be normal to the surface of the target, i.e.,

$$\gamma \equiv 0 \tag{76}$$

In this case, it follows from Eq. (71) that the longitudinal axis of the target at the moment of capture must be directed along the local vertical:

$$\beta_c \equiv \frac{\pi}{2} \tag{77}$$

To find the optimal values of the parameters Δ and a, we introduce two conditions. The first of them is based on the following considerations. After the capture, the target still oscillates under the influence of the gravitational torque, and the angle $\beta = \beta_c = \pi/2$ is an equilibrium position, whereas the angle β_s is an extreme position. Therefore, a quarter of the oscillation period of the target must be equal to the duration of the tether deployment τ_2 (orange curve in Fig. 10), and the first condition can be expressed as

$$\frac{1}{4} T(a, \Delta) = \tau_2(a) \tag{78}$$

where the function $\tau_2(a)$ is obtained from the tug thrust direction optimization (Sec. IV.A).

The second condition is based on the fact that if the material and thickness of the target shell are known, one can determine the momentum of the harpoon required for penetration by either experiment or numerical simulation [16,25]. Therefore, the second condition in dimensionless form can be written as

$$s(a, \Delta) = s_{req} \tag{79}$$

where s_{req} is the required dimensionless initial harpoon momentum, determined from the known required dimensional momentum by analogy with Eq. (69). To find $s(a, \Delta)$, one has to consider Eqs. (68), (70), and (77), which give

$$s = \left| \frac{\beta'_+ - \beta'_-}{\Delta_T \Delta} \right| \tag{80}$$

where, with Eqs. (56), (59), and (77) taken into account,

$$\beta'_+ = -\omega \cos \beta_s \tag{81}$$

$$\beta'_- = \pm \omega \sqrt{\tilde{J} \beta'^2_+ - 2(E_{\beta+} - E_{\beta-})} \tag{82}$$

Here dimensionless quantities β'_-, $E_{\beta-}$ and β'_+, $E_{\beta+}$ are the angular velocity and total energy of the target before and after capture, respectively. The angular velocity β'_- [Eq. (82)] must be taken positive if the target initially rotates in the direction of its mean orbital motion.

The desired parameters a and Δ can be found by solving Eqs. (78) and (79) together with Eqs. (17), (21–23), (63–65), and (80–82) for given geometric and inertial characteristics of the target, its initial total energy $E_{\beta-}$, and required dimensionless momentum of the harpoon s_{req}.

It should be noted that the proposed algorithm for capture optimization is also suitable for assessing the practical feasibility of using the harpoon impact to detumble the particular target. If the value of the parameter Δ obtained from the above equations turns out to be such that the capture point lies outside the target, it means that the initial energy of rotation of the target is too high and, thus, other techniques for detumbling should be used. Mathematically, the condition of applicability of the harpoon impact for the detumbling can be formulated as

$$\Delta \leq \Delta_{max} \tag{83}$$

where Δ is obtained from the optimization algorithm:

$$\Delta_{max} = \left| \frac{2x_2^{max}}{D} \right| \tag{84}$$

Here x_2^{max} is the distance between the center of mass and the most distant point on the sidewall surface of the target where capture is still possible (Fig. 2), and D is the diameter of the target.

V. Numerical Simulations

The objectives of this section are to demonstrate the effectiveness of the proposed algorithms for optimizing the removal process parameters and to assess the influence that the deviations of these parameters from their optimum values have on this process.

To achieve these objectives, three cases will be simulated:

1) In the optimal case, all the recommendations given in Sec. IV are implemented; i.e., the harpoon hits the target at the desired point and, at the end of the tether deployment phase, the tug reaches its optimal position.

2) The harpoon hits the target at the wrong point, but the optimal tug position is reached.

3) The harpoon hits the target at the desired point, but the optimal tug position is not reached.

It is worth mentioning that although the optimization of the removal process is mainly carried out based on approximate equations, the simulations are always performed using the full nonlinear equations. This allows to validate the proposed optimization algorithms.

A. Parameters of the System

For numerical simulations, we choose an Ariane 4 H10 spent upper stage as a target. Its parameters [19] are given in Table 1 along with the tethered towing parameters. Using [25], we assume that to penetrate the aluminum wall of the target, which is 3.5 mm thick, we need the kinetic energy of the harpoon to be about 250 J. Given the kinetic energy and setting the harpoon mass, one can find its required initial speed and, using Eq. (69), the required dimensionless momentum. The parameters of the harpoon are gathered in Table 2.

B. Optimal Case

Using Sec. IV, one can find the optimal parameters of the removal process (Table 3), namely, the orientation of the target at the moment of capture β_c, dimensionless thrust a, capture point shift parameter Δ, thrust direction control parameters [Eq. (75)], and approximate equilibrium positions α_s [Eq. (17)] and β_s [Eq. (22)] of the tether and target, respectively. From the obtained value of the parameter a and the data from Table 1, the tug thrust can be calculated. In the

Table 1 Parameters of the target and tethered towing

Parameter	Value
Target	
Mass m_2	2154 kg
Principal moments of inertia:	
Longitudinal J_x	$3000 \, \text{kg} \cdot \text{m}^2$
Transverse $J_y = J_z$	$28{,}000 \, \text{kg} \cdot \text{m}^2$
Diameter D	2.6 m
Orbit radius r_0	7071 km
Mean motion n	0.00106 rad/s
Initial rotation direction	Opposite to mean motion
Wall material	7020 alloy
Wall thickness	3.5 mm
Initial total dimensionless energy of rotation $E_{\beta-}$	1.0
Dimensionless parameters:	
$\tilde{J} = J_z/(3(J_z - J_x))$	0.373
$\hat{J} = J_z/(m_0 l^2)$	0.0002
$\Delta_T = -D/(2l)$	−0.0013
Tethered towing	
Tug mass m_1	150 kg
Tether length l	1000 m

Table 2 Harpoon parameters

Parameter	Value
Initial kinetic energy KE_h	250 J
Mass m_h	0.1 kg
Initial speed v_h	70.7 m/s
Dimensionless momentum s_{req}	237.8

Table 3 Optimal parameters of the removal process

Parameter	Value
Target orientation at the moment of capture β_c	$\pi/2$ rad
Dimensionless tug thrust $a = P/(lm_1 n^2)$	2.857
Tug thrust P	0.48 N
Capture point shift parameter $\Delta = \Delta_L/\Delta_T$	−3.212
Capture point longitudinal shift $x_2 = \Delta_L l$	4.18 m
Initial tug thrust direction angle η_1	2.47 rad
Final tug thrust direction angle η_2	−1.51 rad
Dimensionless time until tug thrust direction changes τ_1	0.615
Time until tug thrust direction changes $t_1 = \tau_1/n$	9 min 38 s
Dimensionless tether deployment duration τ_2	1.23
Tether deployment duration $t_2 = \tau_2/n$	19 min 17 s
Approximate tether equilibrium position α_s	0.301 rad
Approximate target equilibrium position β_s	0.631 rad

considered case, the thrust is about 0.5 N, which is consistent with the assumption that the orbit of the target remains circular.

When the optimization is complete, the nonlinear equations of the tethered towing can be solved. Figure 9 shows the time histories of the target angular velocity obtained from the full nonlinear Eqs. (3) and (4) as well as from the linearized Eq. (26). There are two clearly visible harmonics in the target oscillations. Their frequencies can be obtained from approximate expressions Eq. (37) and (38). The dimensionless periods of oscillation corresponding to these frequencies are approximately 11 and 0.79. Figure 9 proves that the above approximations are quite suitable for the oscillations obtained by solving the full nonlinear Eqs. (3) and (4).

To estimate the amplitudes of the tether and target oscillations in the optimal case, it is necessary to plot phase diagrams. This is done in the following subsections, where these optimal phase diagrams are given in comparison with the diagrams for nonoptimal cases, in order to more clearly demonstrate the benefits of optimization.

C. Optimal Capture Point Missed

If the optimal tug position is reached, but the harpoon hits the target at the wrong point, the capture point shift Δ is not optimal. Equation (80) shows that in this case the change in angular speed of the target will not be optimal either, because it is proportional to Δ. Figure 10 represents four phase diagrams of the target's attitude motion before, during, and after the capture, corresponding to four values of Δ, one of which is optimal. It can be seen that in any nonoptimal case the target does not reach the desired position β_s within the time τ_2 and has a residual angular speed when the towing starts, which leads to significant oscillations during towing (Fig. 11). Figure 12 represents phase diagrams of relative attitude motion of the tether and the target during towing, which is characterized by the angle $\beta - \alpha$ between the tether and the longitudinal axis of the target, during 30 orbital periods. If the longitudinal shift of the capture point differs strongly from the optimal value, there may be cases when $\beta - \alpha < 0$, and the end face of the target may touch the tether, which will significantly increase the
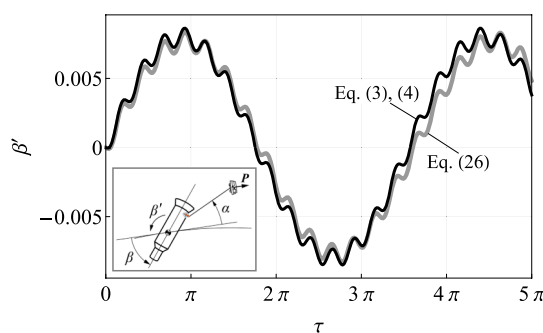
Fig. 9 Time histories of the angular speed of the target [thin black line: Eqs. (3) and (4); thick gray line: Eq. (26)].
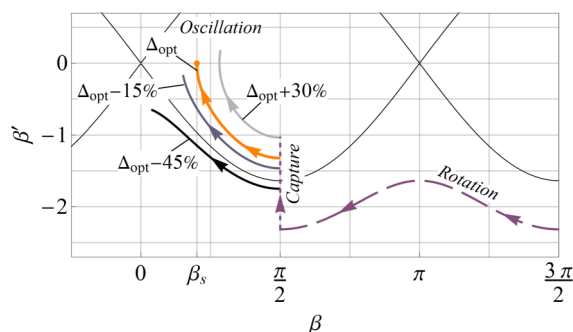
Fig. 10 Phase diagrams of the target's attitude motion before, during, and after the capture.
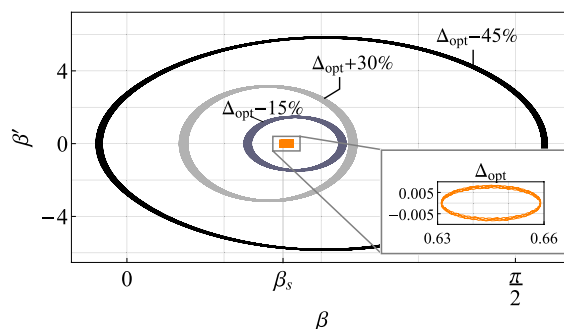
Fig. 11 Phase diagrams of the target's attitude motion during tethered towing.
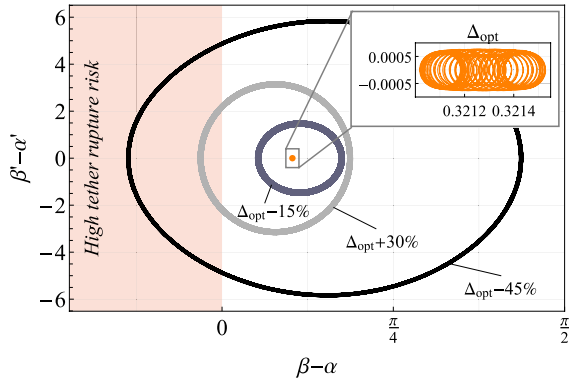
Fig. 12   Phase diagrams of relative attitude motion of the tether and the target during towing.
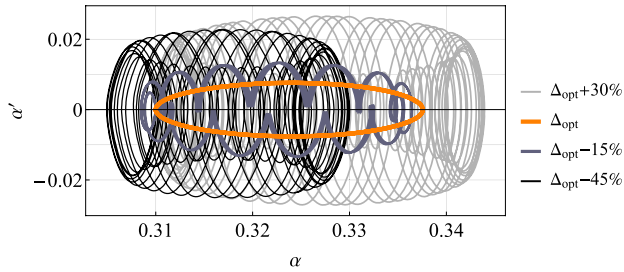

Fig. 13   Phase diagrams of the tether oscillations during towing.
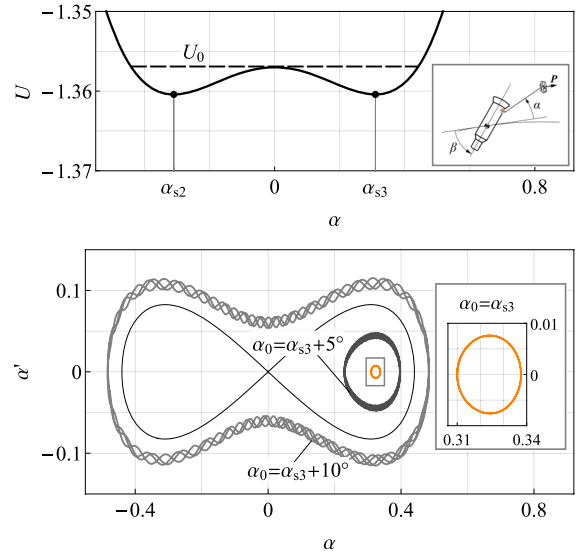

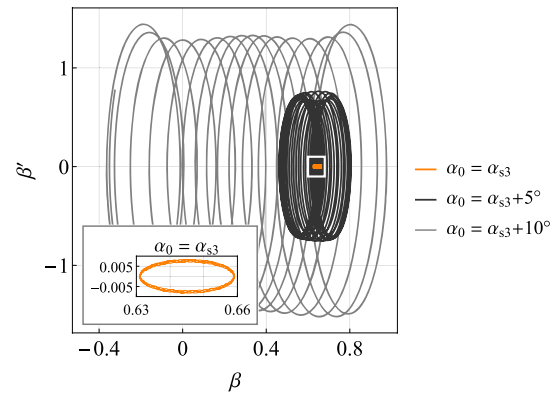Fig. 14   Phase diagrams of the tether oscillations during towing.

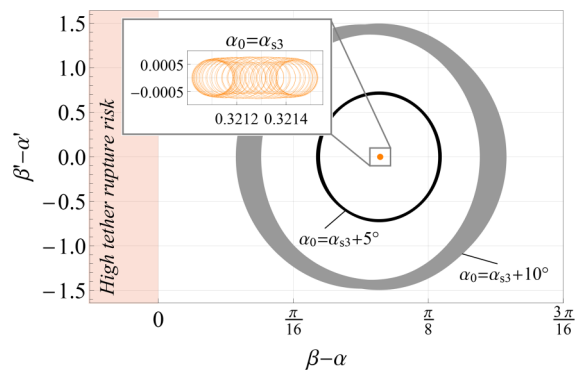Fig. 15   Phase diagrams of the target's attitude motion during tethered towing.

Fig. 16   Phase diagrams of relative attitude motion of the tether and the target during towing.

risk of tether rupture and make the towing unsafe. Note that the undesirable contact between the tether and debris is caused by targeting errors rather than secular effects during towing. For this reason, the accuracy of targeting is crucial.

At the same time, capture errors do not have a significant effect on the tether oscillations during towing, as shown in Fig. 13. Even for the highest of the examined capture errors, the amplitude of the tether oscillations does not exceed 1.2°.

D.   Optimal Tug Position Not Reached

Consider the opposite situation: the harpoon hits the target at the desired point, but the optimal tug position is not reached, i.e., $\alpha_0 \neq \alpha_s$. Let us examine two cases when the tether deviates from the optimal position by 5 and 10°. In the first case, the tether oscillates about the equilibrium position α_{s3} in one of the local potential wells (Fig. 14), which are present if $a < 3$ (Fig. 3). In the second case, the deviation of the initial position of the tether from the optimum value is so large that the tether oscillates about the position $\alpha_{s1} = 0$ despite the presence of the local potential wells. For a better understanding of these situations, a potential energy curve is shown in the upper part of Fig. 14. The value U_0 [Eq. (19)] on this curve corresponds to the separatrix, shown in the lower part of the figure by a black solid line. Finally, the orange curve depicts the phase diagram of the tether oscillations in the optimum case. It can be seen that the amplitude in this case is much smaller. The amplitude of the target's oscillations in the optimal case is also small (less than 0.7°), but the errors in the initial position of the tether can significantly increase it, as shown in Fig. 15. For instance, a 10° deviation of the initial position of the tether from the optimal one increases the amplitude of the target's oscillations up to 40°. However, even in this case, there is no risk of tether rupture, as follows from Fig. 16.

It is of some interest to investigate the contribution of each of two torques acting on the target during towing to its resulting attitude motion. As it was shown in Sec. III.B, with some simplifications it can be assumed that the target oscillations are caused by the torque due to the tether tension $M_t = (1/\hat{J})\Delta_T(\Delta \sin(\alpha - \beta) - \cos(\alpha - \beta))(a \cos \alpha + 3\sin^2 \alpha)$, which is the first term in the right-hand side of Eq. (7), and the gravitational torque $M_g = (1/2\tilde{J}) \sin 2\beta$, which is the second term. Figure 17 represents time histories of these

dimensionless torques for the optimal case as well as for the cases when the optimal tug position is not reached. It is noticeable that in the optimal case both torques are small and almost compensate each other, whereas in the nonoptimal cases the contribution of the torque due to tether tension to the resulting motion is much more significant than the contribution of the gravitational torque.

The numerical simulations have thus shown that the optimization algorithms given in Sec. IV and based on the simplified equations from Sec. III provide that the amplitudes of oscillations of both the tether and the target, calculated using the full nonlinear equations, do not exceed 1°, which will make the tethered towing much easier and safer.
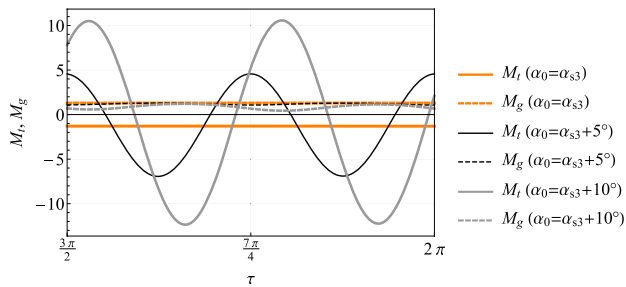
Fig. 17 Dimensionless torques acting on the target during towing: M_t, torque due to the tether tension; M_g, gravitational torque.

VI.   Conclusions

This paper is the first attempt to study as a whole three important consecutive phases of space debris removal involving harpoons: capture, tether deployment, and towing. In addition, it demonstrates the fundamental possibility of detumbling of space debris objects by harpoon impact during the capture phase. A proper selection of the capture parameters and the tug thrust control law during the tether deployment phase can provide small amplitudes of the tether and debris oscillations during towing. The deviations from optimal values of these parameters result in the significant oscillations in the tethered system and increase the risk of tether rupture. The case when the harpoon misses the desired capture point is of special concern.

The future work will focus on certain related issues not covered in this paper. In particular, the initial motion of debris objects can be more general than the motion considered in the presented paper; e.g., the orbit can be elliptical. Further, the kinematic and inertial parameters of debris objects can be known only to a certain degree of accuracy, and the mathematical models should include parameter uncertainty.

Acknowledgment

References

[1] Kessler, D. J., Johnson, N. L., Liou, J., and Matney, M., "The Kessler Syndrome: Implications to Future Space Operations," *Advances in the Astronautical Sciences*, Vol. 137, No. 8, 2010, p. 2010.

[2] Shan, M., Guo, J., and Gill, E., "Review and Comparison of Active Space Debris Capturing and Removal Methods," *Progress in Aerospace Sciences*, Vol. 80, Jan. 2016, pp. 18–32.
https://doi.org/10.1016/j.paerosci.2015.11.001

[3] Hakima, H., and Emami, M. R., "Assessment of Active Methods for Removal of LEO Debris," *Acta Astronautica*, Vol. 144, March 2018, pp. 225–243.
https://doi.org/10.1016/j.actaastro.2017.12.036

[4] Pengyuan, Z., Jinguo, L. I. U., and Chenchen, W. U., "Survey on Research and Development of On-Orbit Active Debris Removal Methods," *Science China Technological Sciences*, Vol. 63, 2020, pp. 2188–2210.
https://doi.org/10.1007/s11431-020-1661-7

[5] Troger, H., Alpatov, A., Beletsky, V., Dranovskii, V., Khoroshilov, V., Pirozhenko, A., and Zakrzhevskii, A., *Dynamics of Tethered Space Systems*, CRC Press, Boca Raton, FL, 2010, pp. 1–22, Chap. 1.

[6] Cartmell, M., and McKenzie, D., "A Review of Space Tether Research," *Progress in Aerospace Sciences*, Vol. 44, No. 1, 2008, pp. 1–21.
https://doi.org/10.1016/j.paerosci.2007.08.002

[7] Aslanov, V. S., and Ledkov, A. S., *Dynamics of Tethered Satellite Systems*, Woodhead Publ. Limited, Cambridge, England, U.K., 2012, pp. 3–102, Chap. 1.

[8] Zhang, F., Sharf, I., Misra, A., and Huang, P., "On-Line Estimation of Inertia Parameters of Space Debris for Its Tether-Assisted Removal," *Acta Astronautica*, Vol. 107, Feb. 2015, pp. 150–162.
https://doi.org/10.1016/j.actaastro.2014.11.016

[9] Aslanov, V. S., "Chaos Behavior of Space Debris During Tethered Tow," *Journal of Guidance, Control, and Dynamics*, Vol. 39, No. 10, 2016, pp. 2399–2405.
https://doi.org/10.2514/1.G001460

[10] Zhong, R., and Zhu, Z. H., "Timescale Separate Optimal Control of Tethered Space-Tug Systems for Space-Debris Removal," *Journal of Guidance, Control, and Dynamics*, Vol. 39, No. 11, 2016, pp. 2540–2545.
https://doi.org/10.2514/1.G001867

[11] Chu, Z., Di, J., and Cui, J., "Analysis of the Effect of Attachment Point Bias During Large Space Debris Removal Using a Tethered Space Tug," *Acta Astronautica*, Vol. 139, Oct. 2017, pp. 34–41.
https://doi.org/10.1016/j.actaastro.2017.06.028

[12] Qi, R., Misra, A. K., and Zuo, Z., "Active Debris Removal Using Double-Tethered Space-Tug System," *Journal of Guidance, Control, and Dynamics*, Vol. 40, No. 3, 2017, pp. 722–730.
https://doi.org/10.2514/1.G000699

[13] Aslanov, V. S., and Yudintsev, V. V., "Chaos in Tethered Tug–Debris System Induced by Attitude Oscillations of Debris," *Journal of Guidance, Control, and Dynamics*, Vol. 42, No. 7, 2019, pp. 1630–1637.
https://doi.org/10.2514/1.G004162

[14] Trivailo, P. M., and Kojima, H., "Dynamics of the Net Systems, Capturing Space Debris," *Transactions of the Japan Society for Aeronautical and Space Sciences, Aerospace Technology Japan*, Vol. 14, No. ists30, 2016, pp. Pr_57–Pr_66.
https://doi.org/10.2322/tastj.14.Pr_57

[15] Botta, E. M., Sharf, I., and Misra, A. K., "Simulation of Tether-Nets for Capture of Space Debris and Small Asteroids," *Acta Astronautica*, Vol. 155, Feb. 2019, pp. 448–461.
https://doi.org/10.1016/j.actaastro.2018.07.046

[16] Dudziak, R., Tuttle, S., and Barraclough, S., "Harpoon Technology Development for the Active Removal of Space Debris," *Advances in Space Research*, Vol. 56, No. 3, 2015, pp. 509–527.
https://doi.org/10.1016/j.asr.2015.04.012

[17] Aglietti, G. S., Taylor, B., Fellowes, S., Salmon, T., Retat, I., Hall, A., Chabot, T., Pisseloup, A., Cox, C., Zarkesh, A., Mafficini, A., Vinkoff, N., Bashford, K., Bernal, C., Chaumette, F., Pollini, A., and Steyn, W. H., "The Active Space Debris Removal Mission Remove Debris. Part 2: In Orbit Operations," *Acta Astronautica*, Vol. 168, March 2020, pp. 310–322.
https://doi.org/10.1016/j.actaastro.2019.09.001

[18] Kang, J., and Zhu, Z. H., "Dynamics and Control of De-Spinning Giant Asteroids by Small Tethered Spacecraft," *Aerospace Science and Technology*, Vol. 94, Nov. 2019, Paper 105394.
https://doi.org/10.1016/j.ast.2019.105394

[19] Gómez, N. O., and Walker, S. J. I., "Eddy Currents Applied to De-Tumbling of Space Debris: Analysis and Validation of Approximate Proposed Methods," *Acta Astronautica*, Vol. 114, Sept. 2015, pp. 34–53.
https://doi.org/10.1016/j.actaastro.2015.04.012.

[20] Kumar, R., and Sedwick, R. J., "Despinning Orbital Debris Before Docking Using Laser Ablation," *Journal of Spacecraft and Rockets*, Vol. 52, No. 4, 2015, pp. 1129–1134.
https://doi.org/10.2514/1.A33183

[21] Pritykin, D., Efimov, S., and Sidorenko, V., "Defunct Satellites in Nearly Polar Orbits: Long-Term Evolution of Attitude Motion," *Open Astronomy*, Vol. 27, No. 1, 2018, pp. 264–277.
https://doi.org/10.1515/astro-2018-0029

[22] Kluever, C. A., *Space Flight Dynamics*, Wiley, Hoboken, NJ, 2018, pp. 275–284, Chap. 8.

[23] Byrd, P. F., and Friedman, M. D., *Handbook of Elliptic Integrals for Engineers and Scientists*, Springer, Berlin, 1971, pp. 15–29, Chap. 2.

[24] Pham, D., and Karaboga, D., *Intelligent Optimisation Techniques: Genetic Algorithms, Tabu Search, Simulated Annealing and Neural Networks*, Springer Science & Business Media, Berlin, 2012, pp. 187–218, Chap. 4.

[25] Virostek, S., Dual, J., and Goldsmith, W., "Direct Force Measurement in Normal and Oblique Impact of Plates by Projectiles," *International Journal of Impact Engineering*, Vol. 6, No. 4, 1987, pp. 247–269.
https://doi.org/10.1016/0734-743X(87)90093-5